

Outflow 20 – 2000 AU from a High-Mass Protostar in W51-IRS2

J. A. Eisner^{1,2,3}, L. J. Greenhill¹, J. R. Herrnstein^{2,4}, J. M. Moran¹, & K. M. Menten^{1,5}

jae@astro.caltech.edu

ABSTRACT

We present the results of the first high angular resolution observations of SiO maser emission towards the star forming region W51-IRS2 made with the Very Large Array (VLA) and Very Long Baseline Array (VLBA). Our images of the H₂O maser emission in W51-IRS2 reveal two maser complexes bracketing the SiO maser source. One of these H₂O maser complexes appears to trace a bow shock whose opening angle is consistent with the opening angle observed in the distribution of SiO maser emission. A comparison of our H₂O maser image with an image constructed from data acquired 19 years earlier clearly shows the persistence and motion of this bow shock. The proper motions correspond to an outflow velocity of 80 km s⁻¹, which is consistent with the data of 19 years ago (that spanned 2 years). We have discovered a two-armed linear structure in the SiO maser emission on scales of ~ 25 AU, and we find a velocity gradient on the order of 0.1 km s⁻¹ AU⁻¹ along the arms. We propose that the SiO maser source traces the limbs of an accelerating bipolar outflow close to an obscured protostar. We estimate that the outflow makes an angle of $< 20^\circ$ with respect to the plane of the sky. Our measurement of the acceleration is consistent with a reported drift in the line-of-sight velocity of the W51 SiO maser source.

Subject headings: ISM: Jets and Outflows – ISM: Kinematics and Dynamics – ISM: Molecules – ISM: Individual (W51) – Masers – Stars: Pre-Main-Sequence

¹Harvard-Smithsonian Center for Astrophysics, 60 Garden Street, Cambridge, MA 02138

²National Radio Astronomy Observatory, P.O. Box 0, Socorro, NM 87801

³Current Address: Palomar Observatory 105-24, California Institute of Technology, Pasadena, CA 91125

⁴Current Address: Renaissance Technologies Corporation, 600 Route 25A, East Setauket, NY 11733

⁵Current Address: Max-Planck-Institut für Radioastronomie, Auf dem Hügel 69, D-53121 Bonn, Germany

1. Introduction

Since the discovery of the first bipolar outflows in star-forming regions (Snell et al. 1980), significant progress has been made in understanding the large-scale characteristics of such outflows (e.g., Bachiller 1996). However, the large columns of gas and dust that obscure massive protostars hinder traditional optical or infra-red observations of at least the inner ~ 100 AU of these outflows, where the exciting protostars reside. This has made it difficult to obtain sufficient data to understand well the process of high-mass star formation. Radio frequency maser emission, which traces velocity coherent clumps of gas entrained in large-scale bulk mass motions, is unattenuated by the neutral gas and dust around massive protostars. Moreover, because masers are compact, high-brightness sources, high angular resolution radio interferometry can be used to probe the structure and kinematics of these outflows on angular scales of $\lesssim 1$ AU for many Galactic sources (e.g., Greenhill et al. 1998; Patel et al. 2000).

Many protostellar outflows exhibit H₂O maser emission at 22 GHz (e.g., Henning et al. 1992; Felli et al. 1992) which traces shocks in dust-laden gas close to the exciting protostars (Elitzur 1992). SiO masers, which are a common feature of late-type stars, are known to occur in only three regions of star formation: W51-IRS2, Sgr-B2 MD5, and Orion-KL (Hasegawa et al. 1986; Snyder & Buhl 1974). Maser action in vibrationally excited states of SiO at 43 GHz requires higher temperatures ($> 10^3$ K) and is more closely associated with exciting sources than is H₂O maser emission (Elitzur 1992). The only non-stellar SiO maser source that has been well studied is the one in Orion-KL, where the maser emission traces an outflow within ~ 100 AU of an obscured massive protostar (Greenhill et al. 1998; Doeleman et al. 1999).

W51-IRS2 is an embedded infrared source ($L_{\text{tot}} \sim 2.8 \times 10^6 L_{\odot}$; Erickson & Tokunaga 1980) in the well-known high-mass star forming region W51. We adopt a distance of 7 kpc to W51 based on maser proper motion studies (Genzel et al. 1981). The region around IRS2 contains an edge-brightened cometary HII region called W51d (Martin 1971; Wood & Churchwell 1989; Gaume et al. 1993) that is associated with a $2.2 \mu\text{m}$ point source (Goldader & Wynn-Williams 1994) and a peak in $12 \mu\text{m}$ emission (Okamoto et al. 2001). An ultra-compact HII region called W51d2 (Martin 1971) is associated with NH₃ and methanol masers (Gaume et al. 1993; Minnier et al. 2001) as well as a feature in the $12 \mu\text{m}$ continuum (Okamoto et al. 2001). W51-IRS2 also contains an H₂O maser complex called W51 North, for which detailed distributions and proper motions have been observed (Schneps et al. 1981), OH maser emission (Gaume & Mutel 1987), and an unresolved SiO maser source (Hasegawa et al. 1986; Ukita et al. 1987; Morita et al. 1992). The strongest H₂O masers, the OH masers, and the SiO masers, are found in a compact region of W51 North termed the “Dominant Center” by Schneps et al. (1981). Although no infrared or radio continuum sources have been detected

within $\sim 2''$ of it (Gaume et al. 1993; Wood & Churchwell 1989; Okamoto et al. 2001), the Dominant Center does coincide with thermal emission from several molecular species including $\text{NH}_3(1,1)$, $\text{NH}_3(2,2)$, $\text{NH}_3(3,3)$, CS, and CH_3CN (Zhang & Ho 1997; Zhang et al. 1998).

The spectrum of the H_2O maser emission covers $V_{\text{LSR}} = -30$ to 130 km s^{-1} , and is peaked around 60 km s^{-1} (Schneps et al. 1981). The SiO emission is peaked around 45 km s^{-1} and covers $V_{\text{LSR}} = 40$ to 50 km s^{-1} , lying within the velocity range of the H_2O maser emission (Morita et al. 1992). The spectra for various molecular species are peaked around $V_{\text{LSR}} \sim 60 \text{ km s}^{-1}$, with typical linewidths of $\sim 20 \text{ km s}^{-1}$ (Zhang & Ho 1997; Zhang et al. 1998).

In this paper, we present the first high angular resolution observations of the SiO maser emission in W51-IRS2. In §2 and §3, we describe interferometric observations of the SiO and H_2O maser emission. We interpret our results in the context of a bipolar outflow model in §4. We also show that previous measurements of the proper motions of H_2O masers and the velocity drifts of SiO masers provide support for our model.

2. Observations and Data Reduction

2.1. VLA Observations and Data Reduction

We observed the $^{28}\text{SiO } v = 2, J = 1 \rightarrow 0$ maser line at 42.820539 GHz, the $6_{1,6} \rightarrow 5_{2,3}$ H_2O maser line at 22.235080 GHz, and continuum emission at 22 and 43 GHz in W51-IRS2. On 1998 March 30, we used the most extended configuration of the VLA of the NRAO,⁶ obtaining an angular resolution of ~ 40 milliarcseconds (at 43 GHz) in 6 hours of on-source integration. We observed in two bands with two sub-arrays, one at 22 and one at 43 GHz. We tuned one 6 MHz band in each sub-array to include a strong maser line, and a second 25 MHz band to line-free continuum. The channel spacing for the line observations was $\sim 0.7 \text{ km s}^{-1}$ at 43 GHz and $\sim 1.3 \text{ km s}^{-1}$ at 22 GHz. The intent of these observations was to establish accurate relative positions among sources at each frequency.

A second observing run, on 1998 July 25, was intended primarily to establish registration of the 22 GHz and 43 GHz images. We observed the SiO and strong H_2O maser lines with the second-most extended configuration of the VLA, and obtained an angular resolution of $\sim 0''.15$ (at 43 GHz). Observing in two bands with two sub-arrays (as above), we “fast-switched” between W51-IRS2 and a calibrator (J1925+2106) with an 80s/80s duty cycle,

⁶The National Radio Astronomy Observatory is a facility of the National Science Foundation operated under cooperative agreement by Associated Universities, Inc.

achieving 40 minutes on-source. We determined the positions of the SiO and strong H₂O maser features with respect to the calibrators to better than 50 mas. We also observed the 22 GHz line-free continuum for ~ 2 hours with two 25 MHz bands (in dual-polarization mode), with the goal of searching for continuum emission associated with the Dominant Center that was not detected on March 30 or by others (Gaume et al. 1993; Wood & Churchwell 1989).

We made images from the data of both observing runs with standard techniques using the NRAO AIPS package (e.g., Rupen 1999). We calibrated the flux scale of the data with observations of 3C286 (which had a flux of 2.52 Jy at 22 GHz and 1.47 Jy at 43 GHz), and determined the bandpass response using NRAO530. For the March 30 observations, we self-calibrated the interferometric data using strong SiO and H₂O maser emission lines at $V_{\text{LSR}} = 50$ and 65 km s⁻¹, respectively. Because the 22 GHz primary beam included W51 North and W51 Main, we mapped both regions together. The gain solutions determined from the strong maser lines were then applied to the rest of the maser emission, as well as to the line-free continuum (e.g., Menten & Reid 1997). By calibrating the continuum in this way, we achieve relative astrometry between the maser and continuum emission that is largely free of systematic effects caused by the troposphere. The registrations of the 22 GHz continuum to the H₂O maser emission and of the 43 GHz continuum to the SiO maser emission are accurate to $\ll 50$ mas, and are largely noise-limited. The registration between the 22 and 43 GHz images is uncertain by $\sim 0''.1$. The formal astrometric position for the SiO maser (the strongest feature at 50 km s⁻¹ on July 25, 1998) is: $(\alpha, \delta)_{\text{J2000}} = (19^{\text{h}}23^{\text{m}}40^{\text{s}}055 \pm 0^{\text{s}}003, 14^{\circ}31'5''59 \pm 0''05)$. We adopt these coordinates as the reference for all relative images presented in this paper.

We deconvolved the point source response from each image and fitted a 2-D elliptical Gaussian to each identified maser spot. (We define a maser “spot” as emission occurring in a given velocity channel. A maser “feature” refers to spots clustered on the sky in $\lesssim 1$ beamwidth, which lie in a contiguous range of channels. Maser features often correspond to physically distinct clumps of gas and separate Doppler components in spectra.) The associated statistical uncertainty in the fitted position of each centroid is $0.5 \times \theta_{\text{beam}}/\text{SNR}$, where SNR is the signal-to-noise ratio, and θ_{beam} is the synthesized half-power beamwidth (Reid & Moran 1988). For these observations, the synthesized beam was $0''.040 \times 0''.039$ with PA= 1° at 43 GHz and $0''.11 \times 0''.09$ with PA= -70° at 22 GHz. We note that the statistical uncertainty applies to largely unresolved or point source emission. It does not apply if there is structure on scales comparable to the beam size, in which case the fitted centroid corresponds to a flux-weighted mean of all the emission regions within the beam.

2.2. VLBA Observations and Data Reduction

On 1994 July 6, we observed the $^{28}\text{SiO } v = 2, J = 1 \rightarrow 0$ maser with the VLBA of the NRAO, integrating approximately 3 hours on-source. At the time of these observations, the array consisted of the Pie Town, Kitt Peak, Los Alamos, Fort Davis, Owens Valley, North Liberty, and Brewster antennas, which afforded an angular resolution of ~ 0.6 mas. We recorded an 8 MHz band and correlated 256 channels (with the correlator in Socorro, NM), which provided a velocity resolution of $\sim 0.2 \text{ km s}^{-1}$.

We calibrated these data with standard techniques of spectral-line VLBI (e.g., Walker 1999; Reid 1999). We achieved an amplitude calibration accurate to approximately 50% using measured system temperatures and *a priori* antenna gains. Global fringe fitting to continuum calibrators (3C273B, 3C345, 3C454.3, J1800+7828, J1740+5211) provided estimates of instrumental delay and fringe rate. We self-calibrated using the peak maser emission at $V_{\text{LSR}} = 43 \text{ km s}^{-1}$, and applied the solutions to the rest of the maser data. As was done for the VLA data, maser spot positions and velocities were determined by fitting 2-D elliptical Gaussian models to maser spots in deconvolved images. The synthesized beam was 0.89×0.52 mas at PA = -38° .

3. Results

3.1. H₂O Masers in W51-IRS2

We imaged seven clusters of H₂O maser emission in W51-IRS2 (with an rms sensitivity of $\sim 5 \text{ mJy}$), and we covered velocities from $V_{\text{LSR}} = 20$ to 100 km s^{-1} (Figures 1 and 2). We note that our velocity coverage does not include the entire spectrum, which extends from $V_{\text{LSR}} \sim -30$ to 130 km s^{-1} (Schneps et al. 1981). One cluster of maser spots is associated with, but offset from, the ultracompact HII region W51d2, and five other clusters of maser spots are coincident with a dense molecular core traced by thermal emission from NH₃(1,1) and other molecular tracers (Figure 1). A seventh cluster (containing only two maser spots) lies between W51d2 and the NH₃ peak. With the exception of the cluster at the northeast corner of the Dominant Center region and the cluster between W51d2 and the NH₃ emission peak, all were previously observed by Schneps et al. (1981). A comparison of our image with Schneps et al. (1981) reveals a remarkable stability in the structure of the H₂O maser source over a 19 year baseline (Figure 3). In the remainder of this discussion, we will focus on the H₂O maser clusters labeled \mathcal{A} and \mathcal{B} in Figure 3.

The strongest water maser emission in the Dominant Center \mathcal{A} , the SiO maser source,

and the apparent vertex of the central cluster of H₂O maser spots \mathcal{B} are approximately colinear on the sky. The position angle of this line is $\sim 108^\circ$, and the distance between \mathcal{A} and \mathcal{B} is ~ 4270 AU (assuming a distance of ~ 7 kpc). Schneps et al. (1981) measured proper motions of the H₂O masers from 1977 to 1979 that indicate that \mathcal{A} and \mathcal{B} (denoted “NW Cluster” and “Dominant Center Reference” in their paper) are moving away from each other in the plane of the sky at $v = 160 \pm 40$ km s⁻¹ along this position angle. (We estimated the uncertainty in this determination from the dispersion in the proper motions of five maser spots in the Dominant Center Reference cluster from the data in Schneps et al.) We confirm the proper motion by comparing the separation of clusters \mathcal{A} and \mathcal{B} from Schneps et al. (1981) to the separation measured by us 19 years later (Figure 3). We measure an increase of separation from 0^{''}52 to 0^{''}61 and find $v \sim 150$ km s⁻¹, which is consistent with Schneps et al. (1981). Imai et al. (2001) present an independent estimate of the proper motions based on recent short time-baseline VLBA observations, and report a relative velocity between \mathcal{A} and \mathcal{B} of ~ 200 km s⁻¹ (Imai et al. 2001).

In addition to confirming the \mathcal{A} - \mathcal{B} proper motion measured by Schneps et al. (1981), our observations show that the H₂O maser structures retained their shapes as they moved apart. Specifically, as shown in Figure 3, the structures of \mathcal{A} and \mathcal{B} have not changed significantly over the 19 years. (Slight discrepancies between the two images can be partially attributed to the fact that Schneps et al. (1981) covered velocities from -10 to 80 km s⁻¹, while the observations presented here covered velocities from 20 to 100 km s⁻¹.) This is particularly noteworthy because the distribution of H₂O masers in cluster \mathcal{B} suggests that it traces the limb of a bow shock, and we actually see this bow shock moving persistently outward over a 19 year interval.

3.2. SiO Maser Source

The SiO maser emission lies in between the H₂O maser complexes \mathcal{A} and \mathcal{B} on the sky and is effectively coincident with the peak of thermal NH₃ emission (Figure 1). The spectrum of the SiO maser emission covers velocities from $V_{\text{LSR}} = 38$ to 60 km s⁻¹, which lie within the velocity extent of the H₂O maser emission (Figure 2), but are offset from the peak of thermal emission from NH₃ (and other molecular tracers) at ~ 60 km s⁻¹ (Zhang & Ho 1995; Zhang et al. 1998).

We resolved the angular structure of the W51-IRS2 SiO maser source with both the VLA and the VLBA data. The source has a linear structure with a position angle of $\sim 105^\circ$ (Figures 4 and 5). The SiO maser also shows an apparent gradient in line-of-sight (LOS) velocity with position, with redder spots to the west and bluer spots to the east. From the

data shown in Figures 4 and 5, we estimate this gradient to be $\sim 1 \text{ km s}^{-1} \text{ mas}^{-1}$ ($\sim 0.1 \text{ km s}^{-1} \text{ AU}^{-1}$). The SiO maser emission seems to be distributed along a northern and a southern “arm”, and the LOS velocities of the two arms are offset by 5 to 10 km s^{-1} (Figure 5).

The VLA image is more sensitive to the large scale structure in the SiO maser source but less accurate in pinpointing emission centers than the VLBA. Specifically, the rms sensitivities are 7 mJy for the VLA and 14 mJy for the VLBA, while the angular resolutions are $\sim 40 \text{ mas}$ and $\sim 0.6 \text{ mas}$, respectively. Thus, while the observed emission in the VLA image may be a flux-weighted centroid of structures smaller than the beamsize, the VLBA image reveals the positions of the compact core components. The total flux in the VLBA spectrum is considerably less than that of the VLA spectrum (Figure 2), which is probably due to the different instrument resolutions and/or source variability.

3.3. Continuum Emission

Figure 1 shows the radio continuum emission in the vicinity of W51-IRS2. Detection of W51d and W51d2 is consistent with previous observations (Gaume et al. 1993; Wood & Churchwell 1989). We did not detect any radio continuum emission in the Dominant Center region, setting an upper limit of $\sim 0.1 \text{ mJy}$ at 22 GHz (as compared to the previous upper limit of $\sim 1 \text{ mJy}$; Gaume et al. 1993). The lack of radio continuum emission in a dense molecular core traced by maser emission and thermal NH_3 emission indicates that any compact optically thick HII region in the Dominant Center is too small to be detected (i.e. $\lesssim 50 \text{ AU}$ at 10^4 K), perhaps due to confinement by accretion from the surrounding molecular cloud (e.g., Osorio et al. 1999) or by outflow (or both).

4. Discussion: Outflow in the Dominant Center Region

The positional coincidence and velocity overlap of the SiO and H_2O maser emission with a peak in the thermal NH_3 emission (Figures 1 and 2) probably signifies that the masers trace star forming activity in the denser portions of a molecular cloud core. The outflowing motions of the H_2O masers on scales of $\sim 4200 \text{ AU}$ and the apparent bow shock structure \mathcal{B} also support this conclusion.

We suggest that the SiO maser source in W51-IRS2 marks the position of a massive protostar, because of excitation requirements of the $v = 2, J = 1 \rightarrow 0$ SiO maser emission ($n_{\text{H}_2} \sim 10^{10} \text{ cm}^{-3}$, $T_{\text{ex}} \sim 3500 \text{ K}$; Elitzur 1992). Thus, the absolute position of the protostar is within 5 mas of our reference VLA SiO astrometric position, $(\alpha, \delta)_{\text{J2000}} = (19^{\text{h}}23^{\text{m}}40^{\text{s}}.055 \pm$

0^s003, 14^o31'5''59 ± 0''05). We surmise that the exciting protostar is massive based on an estimate of the mechanical luminosity of the H₂O maser outflow: assuming an H₂ density for the outflow of $\geq 10^6 \text{ cm}^{-3}$ (realistic based on the H₂O and OH maser emission in the vicinity; Elitzur 1992), an opening angle of 25°, and flow velocity of $\sim 80 \text{ km s}^{-1}$, we find $L \geq 10 L_{\odot}$.

The two-armed linear structure of the SiO maser is suggestive of a diverging outflow on scales $\lesssim 25 \text{ AU}$ (Figure 5). We propose that the SiO maser emission may trace the limbs of a rotating conical bipolar outflow from a massive protostar. In the context of this model, we can localize the relative position of the exciting protostar on very small scales. Specifically, we speculate that the protostar lies within several AU ($\sim 5 \text{ mas}$) of the intersection of the northern and southern limbs (although the absolute position is known to only $\sim 50 \text{ mas}$).

The velocity gradient of the SiO maser emission, present along the northern (blue) arm and the southern (red) arm (Figure 5), implies acceleration along the putative outflow. This acceleration is also visible in the VLA image (Figure 4), which shows bluer emission to the east and redder emission to the west, as expected. However, the VLA and VLBA data both show some blue emission that is inconsistent with the fitted acceleration of $\sim 1 \text{ km s}^{-1} \text{ mas}^{-1}$. We suggest that this emission may not be associated with the proposed diverging outflow, but it may instead be associated with a separate dynamical component (e.g., a disk or associated wind, as in Hollenbach et al. 1994).

The outflow traced on small scales by SiO maser emission appears to be reflected on large scales by the H₂O maser complexes \mathcal{A} and \mathcal{B} . The position angle on the sky of the SiO outflow ($\sim 105^\circ$) is consistent with the angle of the outflow traced by the motions and positions of clusters \mathcal{A} and \mathcal{B} (Figure 3). The bow shock H₂O maser structure \mathcal{B} subtends the same opening angle as the SiO maser emission ($\sim 25^\circ$; Figures 3 and 5). Although \mathcal{A} does not show a clear bowshock morphology (perhaps due to inhomogeneities or gradients in the ambient medium), the angle subtended by the strongest H₂O maser emission in \mathcal{A} is consistent with the proposed outflow. The H₂O maser emission also shows the same general trend in LOS velocity as the SiO maser emission, with bluer emission to the east and redder emission to the west. Thus, it appears that the SiO maser emission traces the limbs of a collimated diverging conical flow close to the exciting source, while the H₂O masers trace the shocks that form where the ballistic outflow runs into ambient material. (We note that the ultracompact HII region W51d has a bowshock morphology whose position angle is close to that of the H₂O outflow and bowshock, which may be a coincidence or may be indicative of a larger scale outflow from the Dominant center region along the same position angle.)

We estimate the angle of the putative outflow with respect to the plane of the sky, θ , by comparing the proper motions and line-of-sight velocities of the H₂O maser complexes \mathcal{A}

and \mathcal{B} :

$$\theta = \tan^{-1}(v_{\text{LOS}}/v_{\text{prop}}) \sim 4^\circ, \quad (1)$$

where $v_{\text{LOS}} = 5 \text{ km s}^{-1}$ is half the difference in LOS velocity between \mathcal{A} and \mathcal{B} and $v_{\text{prop}} = 80 \text{ km s}^{-1}$ is half the speed at which \mathcal{A} and \mathcal{B} are separating on the sky. However, because of the large dispersion in the LOS velocities of H_2O maser clusters \mathcal{A} and \mathcal{B} , this is only a rough estimate.

We may also estimate θ by combining LOS velocity information from the SiO maser emission with the proper motions of the H_2O maser emission. For purposes of discussion, we assume a common acceleration. On small scales the acceleration is given by $a_1 = v_{\text{SiO}}^2/2d_{\text{SiO}} = (v_1^2 \cos \theta)/(2d_1 \sin^2 \theta)$. Here, $d_1 = 30 \text{ AU}$ (4 mas) is the measured transverse distance from the intersection of the two arms to the easternmost maser spot in Figure 5, and $v_1 = 4 \text{ km s}^{-1}$ is the measured difference in line-of-sight velocity between these features. On larger scales, the acceleration is given by $a_2 = v_{\text{H}_2\text{O}}^2/2d_{\text{H}_2\text{O}} = (v_2^2)/(2d_2 \cos \theta)$, where $d_2 = 2130 \text{ AU}$ ($0''.6$) and $v_2 = 80 \text{ km s}^{-1}$ are the transverse separation and transverse velocity difference of the SiO maser and H_2O maser complexes \mathcal{A} and \mathcal{B} (where we assume that the transverse velocity of the SiO maser is effectively 0). If $a_1 = a_2$, then the angle of the outflow is given by

$$\theta = \tan^{-1} \left(\frac{v_1}{v_2} \sqrt{\frac{d_2}{d_1}} \right) \sim 20^\circ. \quad (2)$$

However, a constant acceleration over $\sim 2200 \text{ AU}$ is unlikely to occur. For a decelerating flow, $a_1 > a_2$ and $\theta < 20^\circ$. If we assume constant acceleration of the jet out to d_1 with no acceleration thereafter, we obtain $\theta = \tan^{-1}(v_1/v_2) \sim 3^\circ$, consistent with the value estimated from Equation 1. Thus, the outflow probably lies within 20° of the plane of the sky.

For the simple case of constant acceleration, we estimate the acceleration of the outflow to be $0.5 \text{ km s}^{-1} \text{ yr}^{-1}$, which gives a line-of-sight acceleration of $0.2 \text{ km s}^{-1} \text{ yr}^{-1}$. For a decelerating flow, the implied acceleration on the scale of the SiO maser emission is larger. This is consistent with a $0.4 \text{ km s}^{-1} \text{ yr}^{-1}$ drift in the line-of-sight velocity of individual SiO maser spectral features reported by Fuente et al. (1989). However, the velocities of spectral components measured by others after 1989 (Hasegawa et al. 1986; Morita et al. 1992; this work) are not entirely consistent with the trend fit by Fuente et al. (1989), and the fluxes of components vary by over an order of magnitude from observation to observation. Although suggestive, we conclude that the estimated acceleration from Fuente et al. should be treated with caution.

Using our estimate of the angle of the outflow with respect to the plane of the sky, we can also make an order of magnitude estimate of the mass loss rate for the putative protostar. Assuming that the outflow consists primarily of molecular hydrogen with a density

of $n_{H_2} \sim 10^9 \text{ cm}^{-3}$ (reasonable for SiO maser excitation; Elitzur 1992), we find

$$\dot{M} \geq \frac{m_p n \pi h^2 v_1}{2 \sin \theta} \sim 10^{-6} M_\odot \text{ yr}^{-1}. \quad (3)$$

Here, m_p is a proton mass, $h = 21 \text{ AU}$ is the distance between the two limbs of SiO maser emission measured at the easternmost maser spot in Figure 5, $v_1 = 4 \text{ km s}^{-1}$ is defined above, and $\theta = 20^\circ$ is the upper limit on the angle of the outflow with respect to the plane of the sky under the assumption of constant acceleration. We note that our estimate is consistent with those for other massive protostars, $\sim 10^{-6} M_\odot \text{ yr}^{-1}$ (e.g., Lada 1985).

We estimate the line-of-sight velocity of the exciting protostar by averaging the velocities of the SiO maser features on the north and south limbs of the outflow: $v_* \sim 47 \text{ km s}^{-1}$. This is significantly different than the 60 km s^{-1} systemic velocity of the dominant center region obtained from interferometric observations of thermal NH_3 emission (Zhang & Ho 1995; Ho et al. 1983). However, the linewidth of the thermal NH_3 emission is $\sim 20 \text{ km s}^{-1}$, and the angular resolution of the NH_3 observations is $1''$. Thus, it is possible that the molecular core has several components (possibly marked by the other clusters of H_2O maser emission in the Dominant Center region), which are moving at different LOS velocities, and perhaps the protostar that is driving the outflow discussed here is associated with one of these components.

We postulate that the conical outflow rotates (counterclockwise) about the axis of outward flow in order to explain the $\sim 5 \text{ km s}^{-1}$ difference in LOS velocity between the north and south limbs of SiO maser emission seen in Figure 5. The ratio of transverse to rotational energy is $(v_{\text{flow}}/v_{\text{rot}})^2 \sim (80/2.5)^2 \sim 1000$ — i.e., most of the kinetic energy is in the outward flow component. Rotating bipolar outflows have been theorized to occur due to “X-winds” where magnetocentrifugal effects drive the outflow (Najita 1995; Shu et al. 1994), or due to the interaction of a spherical protostellar wind with a time-dependent infall from a parent molecular cloud (Wilkin & Stahler 1998). The limbs are presumably a preferred site of maser emission because the longer path lengths and the similarity of projected LOS velocities result in greater amplification. The limbs of a conical bipolar outflow traced by SiO masers have also been observed in Orion-KL, though without rotation (Greenhill et al. 1998).

Instead of a conical flow, the two arms of SiO maser emission in W51 could also indicate the presence of two protostars, possibly comprising a close binary system, wherein the north and south arms trace two separate outflows. While this model can also explain our results, the coincidence of the opening angle of the SiO maser emission with the angle subtended by the bow shock structure leads us to favor the conical outflow model.

We also consider a precessing jet model. Were the precessing jet to behave like a rigid rod, then magnetic coupling to ionized ambient material might account for the observed

velocity structure of the SiO maser emission. However, it is more likely that such a jet would instead be ballistic, in which case the precession cone of the jet would have no “limbs” where the observed path length is greatest. In this case, if the jet comprises knots or bullets of material, visible emission would appear to “fill” the precession cone, something we do not see. A possible “fix” is if the precessing jet shocks SiO in a rotating “cocoon” of gas, exciting maser emission. If the decay time for emission of shocked gas is long compared to the precession time-scale of the jet, this model would lead to observed SiO maser emission identical to the rotating conical outflow model. If this model is correct, then it should be possible to detect periodic changes in the brightness of the arms of SiO maser emission detected with the VLBA. The variations in brightness of the two arms should be out of phase.

5. Conclusions

We have resolved the structure of the W51-IRS2 SiO maser source, and linked it to a protostellar outflow associated with two long-known sites of intense H₂O maser emission. We propose that the masers trace an accelerating bipolar protostellar outflow inclined $< 20^\circ$ with respect to the plane of the sky, which may detectably rotate about the axis of flow within tens of AU of the protostar. We estimate the position angle of the flow to be $\sim 105^\circ$ up to 4200 AU from the central star. The proper motions of H₂O maser clusters bracketing the SiO maser source indicate an outflow velocity of $\sim 80 \text{ km s}^{-1}$ along this position angle, and one of these clusters appears to trace a bow shock that subtends an angle consistent with the opening angle suggested by the two limbs of SiO maser emission. We estimate the acceleration of the outflow to be $\sim 0.5 \text{ km s}^{-1} \text{ yr}^{-1}$, which is consistent with the $0.4 \text{ km s}^{-1} \text{ yr}^{-1}$ line-of-sight velocity drift measured by Fuente et al. (1989).

In the larger context, this bipolar flow lies in within a $\sim 10^4$ AU cloud core hosting multiple centers of H₂O maser emission. The outflow does not extend to the limits of the core or to the other centers of H₂O maser emission. We estimate the line-of-sight velocity of the protostar that is driving the bipolar outflow to be $\sim 47 \text{ km s}^{-1}$, significantly different than the systemic velocity of the NH₃ core (60 km s^{-1}). We suggest that there may be several star-forming fragments within this core, perhaps marked by the other centers of H₂O maser activity.

REFERENCES

Bachiller, R. 1986, ARA&A, 34, 111

- Doeleman, S.S., Lonsdale, C.J., & Pelkey, S. 1999, *Ap. J.*, 510, L55
- Elitzur, M. 1992, *Astronomical Masers* (Dordrecht: Kluwer)
- Erickson, E.F., & Tokunaga, A.T. 1980, *Ap. J.*, 238, 596
- Felli, M., Palagi, F., & Tofani, G. 1992, *A&A*, 255, 293
- Fuente, A., Martin-Pintado, J., Alcolea, J., & Barcia, A. 1989, *A&A*, 223, 321
- Gaume, R., Johnston, K.J., & Wilson, T.L. 1993, *Ap. J.*, 417, 645
- Gaume, R., & Mutel, R.L. 1987, *ApJS*, 65, 193
- Genzel, R., Becklin, E.E., Wynn-Williams, C.G., Moran, J.M., Reid, M.J., Jaffe, D.T., & Downes, D. 1982, *Ap. J.*, 255, 527
- Genzel, R., et al. 1981, *Ap. J.*, 147, 1039
- Greenhill, L.J., Gwinn, C.R., Schwartz, C., Moran, J.M., & Diamond, P.J. 1998, *Nature*, 396, 650
- Goldader, J.D., & Wynn-Williams, C.G. 1994, *Ap. J.*, 433, 164
- Hasegawa, T., Morita, K., Okumura, S., Kaifu, N., Suzuki, H., Ohishi, M., Hayashi, M., Ukita, N. 1986, in *Masers, Molecules, and Mass Outflows in Star Forming Regions*, ed. A.D. Haschick (Westford: Haystack), 275
- Henning, T., Cesaroni, R., Walmsley, M., & Pfau, W. 1992, *A&AS*, 93, 525
- Ho, P.T.P., Genzel, R., & Das, A. 1983, *Ap. J.*, 266, 596
- Hollenbach, D., Johnstone, D., Lizano, S., & Shu, F. 1994, *Ap. J.*, 428, 654
- Imai, H., Sasao, T., Kameya, O., Watanabe, T., Omadaku, T., Nishio, M., Asaki, Y., & Nakajima, J. 2001, in *Cosmic Masers*, Proc. IAU Symp 206, ed. V. Migenes (San Francisco: ASP), in press
- Lada, C.J. 1985, *ARA&A*, 23, 267
- Martin, A. 1972, *M.N.R.A.S.*, 157, 31
- Menten, K.M., & Reid, M.J. 1997, *Ap. J.*, 476, 327
- Minnier, V., Conway, J.E., & Booth, R.S. 2001, *A&A*, 369, 278

- Morita, K-I., Hasegawa, T., Ukita, N., Okumura, S.K., & Ishiguro, M. 1992, PASJ, 44, 373
- Najita, J. 1995, Rev. Mex. A.A., 1, 293
- Okamoto, Y.K., Kataza, H., Yamashita, T., Miyata, T., & Onaka, T. 2001, Ap. J., 553, 254
- Osorio, M., Lizano, S., & D'Alessio, P. 1999, Ap. J., 525, 808
- Patel, N.A., Greenhill, L.J., Herrnstein, J.R., Zhang, Q., Moran, J.M., Ho, P.T.P., & Goldsmith, P.F. 2000, Ap. J., 538, 268
- Reid, M.J. 1999, in ASP Conf. Ser. 180, Synthesis Imaging in Radio Astronomy II, ed. G.B. Taylor, C.L. Carilli, & R.A. Perley (San Francisco: ASP), 481
- Reid, M.J., & Moran, J.M. 1988, in Galactic and Extragalactic Radio Astronomy, ed. G.L. Verschuur, & K.I. Kellerman (Berlin: Springer-Verlag)
- Rupen, M.P. 1999, in ASP Conf. Ser. 180, Synthesis Imaging in Radio Astronomy II, ed. G.B. Taylor, C.L. Carilli, & R.A. Perley (San Francisco: ASP), 481
- Schneps, M.H., Lane, A.P., Downes, D., Moran, J.M., Genzel, R., & Reid, M.J. 1981, Ap. J., 249, 124
- Schwartz, R.D., & Greene, T.P. 1999, AJ, 117, 456
- Shu, F.H., Najita, J., Ostriker, E., Wilkin, F., Ruden, S., & Lizano, S. 1994, Ap. J., 429, 781
- Snell, R.J., Loren, R.B., & Plambeck, R.L. 1980, Ap. J., 239, L17
- Snyder, L.E., & Buhl, D. 1974, Ap. J., 189, L31
- Ukita, S., Hasegawa, T., Kaifu, N., Morita, K.-I., Okumura, S., Suzuki, H., Ohishi, M., & Hayashi, M. 1987, in Star Forming Regions, IAU Symp. No. 115, ed. M. Peimbert, & J. Jugaku (Dordrecht: Reidel), 178
- Walker, R.C. 1999, in ASP Conf. Ser. 180, Synthesis Imaging in Radio Astronomy II, ed. G.B. Taylor, C.L. Carilli, & R.A. Perley (San Francisco: ASP), 481
- Wilkin, F.P., & Stahler, S.W. 1998, Ap. J., 502, 661
- Wood, D.O.S., & Churchwell, E. 1989, Ap. J., 69, 831
- Zhang, Q., Ho, P.T.P., & Ohashi, N. 1998, Ap. J., 494, 636

Zhang, Q., & Ho, P.T.P. 1997, Ap. J., 488, 241

Zhang, Q., & Ho, P.T.P. 1995, Ap. J., 450, L63

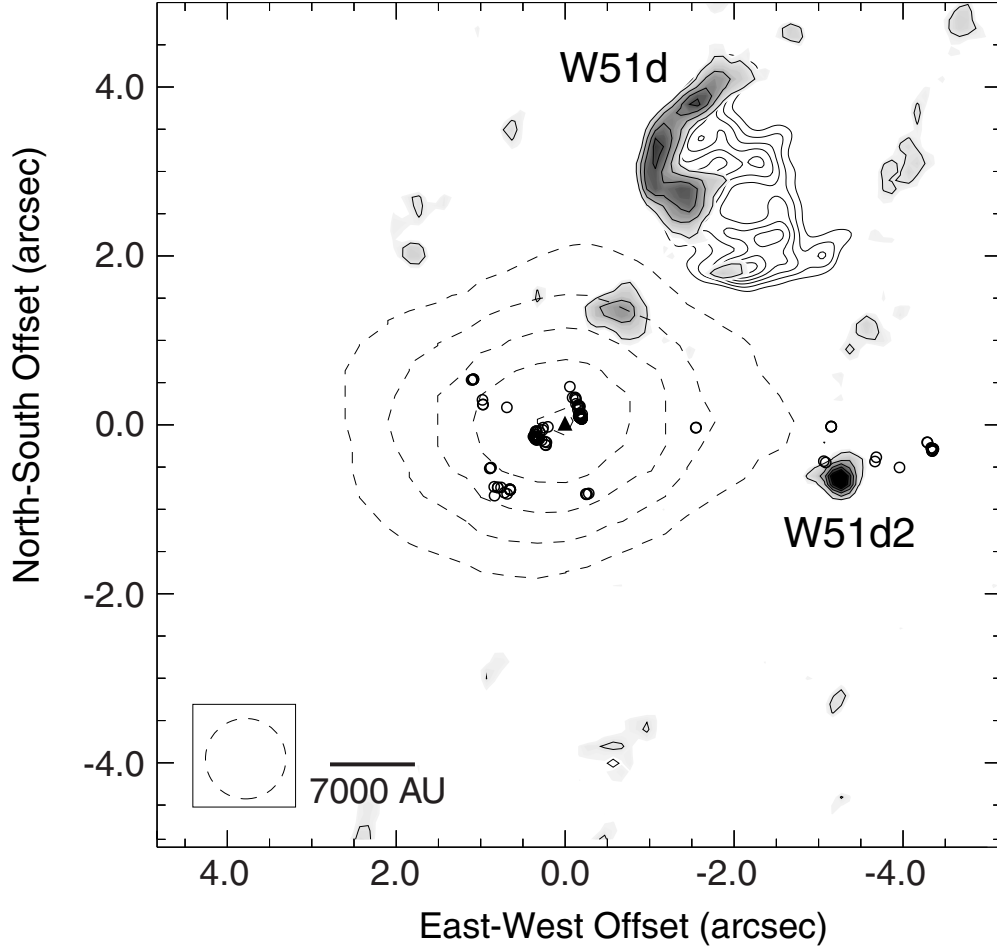


Fig. 1.— The W51-IRS2 star forming region, mapped with the VLA. The coordinates are offset from the position of the SiO maser source (indicated by the black triangle) at $(\alpha, \delta)_{J2000} = (19^{\text{h}}23^{\text{m}}40^{\text{s}}055 \pm 0^{\text{s}}004, 14^{\circ}31'5''59 \pm 0''07)$. The continuous contours represent continuum emission at 22 GHz observed with $0''.24$ resolution (filled contours starting at 8 mJy, separated by 4 mJy), and observed at $0''.47$ resolution (unfilled contours starting at 8 mJy, separated by 1.7 mJy). The rms noise levels are 1.0 mJy and 1.7 mJy, respectively. The dashed contours represent thermal emission from the $(J, K) = (1, 1)$ transition in NH_3 observed with $\sim 1''$ resolution (Zhang & Ho 1997). The open circles indicate H_2O maser emission (at 22 GHz), and the triangle represents the position of the SiO maser source (at 43 GHz). The previously identified sources W51d and W51d2 are labeled. The relative astrometry of SiO masers, H_2O masers, and 22 GHz continuum sources is accurate to $\lesssim 0''.1$.

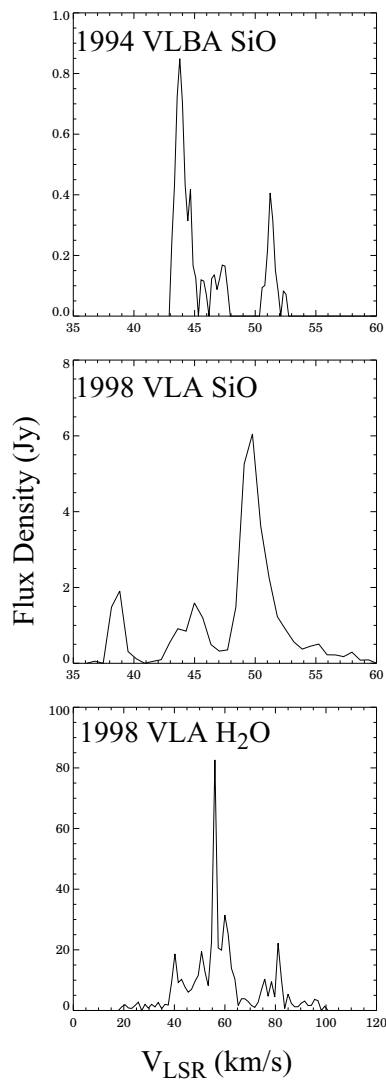


Fig. 2.— (top) Spectrum of the SiO maser emission observed on 1994 July 6 with the VLBA, (middle) and on 1998 March 30 with the VLA. Note that the flux in the VLBA spectrum is much less than the VLA spectrum, in part because the former is sensitive to only the very small scale emission. (bottom) Band-limited spectrum of the H₂O maser emission observed on 1998 March 30 with the VLA. Emission has been observed previously over a broader velocity range, -30 to 130 km s⁻¹ (Schneps et al. 1981).

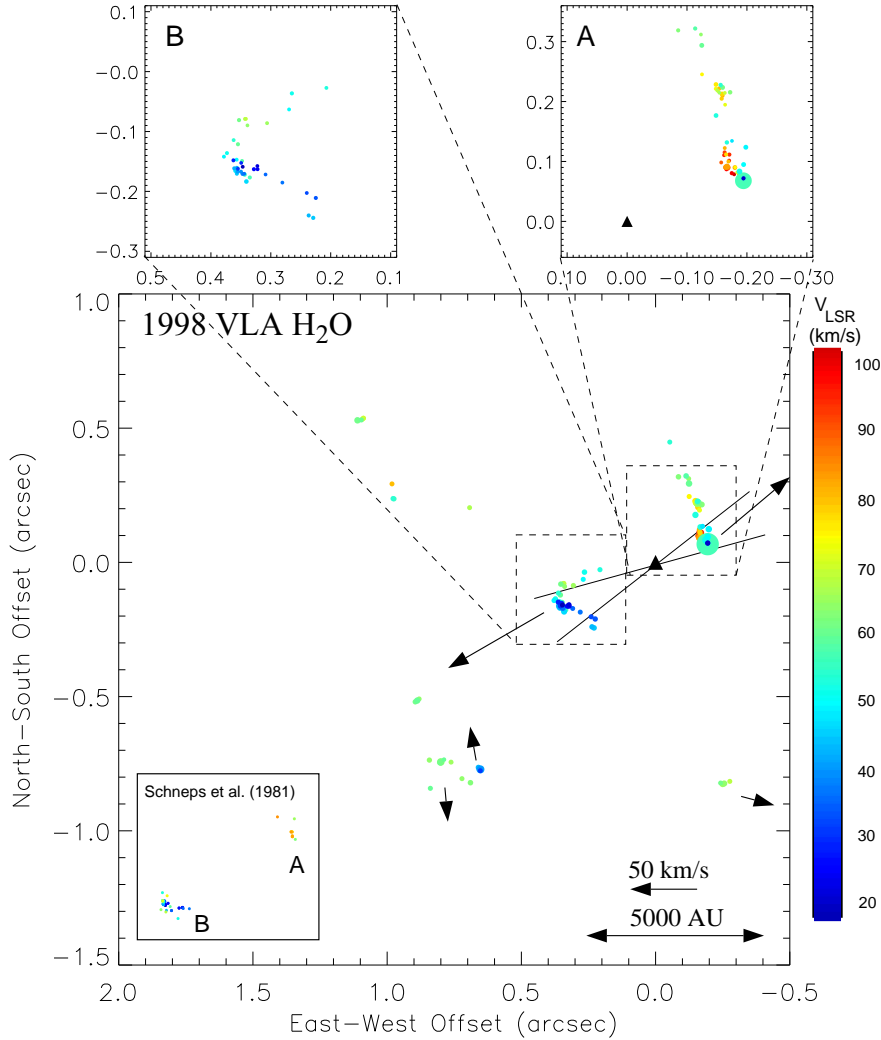


Fig. 3.— The distribution of H_2O maser emission in the Dominant Center Region, observed with the VLA on 1998 March 30. The coordinates are offset from the VLA astrometric position of the SiO maser source (indicated by the black triangle) at $(\alpha, \delta)_{\text{J2000}} = (19^{\text{h}}23^{\text{m}}40^{\text{s}}055, 14^{\circ}31'5''59)$. The circles represent H_2O maser spots, where color indicates line-of-sight velocity and area is proportional to flux density. The uncertainties in the relative fitted positions of the maser spots are smaller than the sizes of the plotted symbols. The registration error of this map with respect to the SiO reference position is $0''.07$ in each coordinate. The arrows denote average measured proper motions of the clusters of H_2O masers measured with data from 1979 (Schneps et al. 1981). The opening angle of the SiO maser emission seen in Figure 5 has been extrapolated to the scales of the H_2O maser emission (solid lines). Blow-ups of two clusters of masers, denoted \mathcal{A} and \mathcal{B} are shown at the top. The inset shows the maser distributions of \mathcal{A} and \mathcal{B} in 1979.

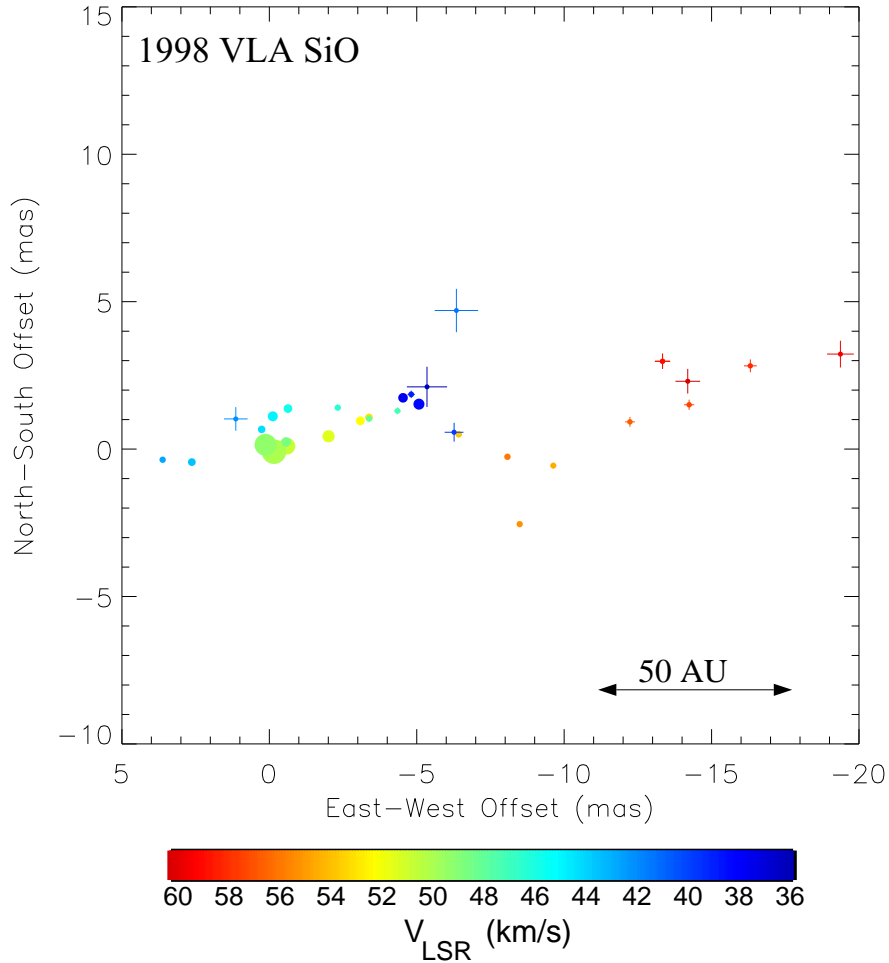


Fig. 4.— The W51-IRS2 SiO maser source, mapped with the VLA at 40 mas resolution on 1998 March 30. The coordinates in this figure are offset from $(\alpha, \delta)_{\text{J2000}} = (19^{\text{h}}23^{\text{m}}40^{\text{s}}055, 14^{\circ}31'5''59)$. These coordinates correspond to the black triangle plotted in Figures 1 and 3. The absolute registration of the image is accurate to 50 mas in each coordinate. The circles represent individual maser spots, where the color corresponds to line-of-sight velocity, and area is proportional to flux density. Error bars denote 1σ uncertainties in relative position for the emission centroid at each velocity. Note the narrower velocity range here compared to Figure 3.

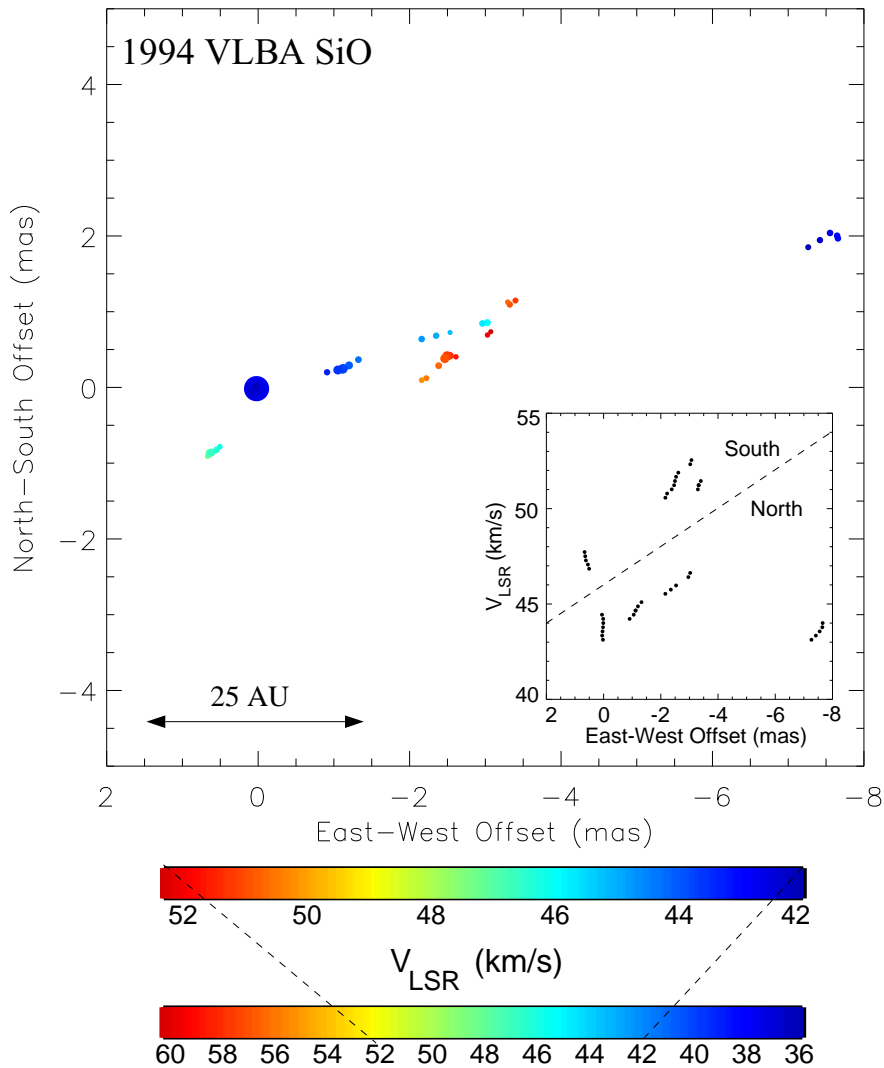


Fig. 5.— The W51-IRS2 SiO maser source, mapped with the VLBA at 0.48 mas resolution, on 1994 July 6. The coordinate offsets are with respect to the strongest emission at the time of observation. No VLBA astrometric data were available to register this image with the one in Figure 4. However, by inspection, the images in Figures 4 and 5 are probably registered to within ~ 1 mas. In the context of our model the protostar would lie at about the position $(-5, +1)$ mas in both images. The position uncertainties are all smaller than the sizes of the plotted symbols. Color corresponds to line-of-sight velocity, and the areas of the plotted symbols are proportional to flux density. We plot the color bar from Figure 4 beneath the color bar for this image to permit ready comparison. The inset shows the LSR velocity of the SiO maser spots versus east-west offset. The dashed line denotes a slope of $1 \text{ km s}^{-1} \text{ mas}^{-1}$.